Mechanical Properties of Soda Lime Glass

Nicholas G. Rudawski

MSE 365

Tuesday Laboratory Section

Friday, January 30th, 2004

1. Abstract

The mechanical properties of soda lime glass have been investigated by performing flexural testing, conducting two-parameter Weibull analyses, analyzing the fracture surfaces of failed samples using scanning electron and optical microscopy, and performing Vickers indentations to determine fracture toughness and analyze residual stress fields. For as-received, 240 grit abraded, and 1200 grit abraded rods, Weibull analysis yielded characteristic strengths of 191, 65.1, and 172 MPa respectively with Weibull moduli of 5.12 ± 0.07, 9.10 ± 0.25, and 5.44 ± 0.14 respectively. The larger values of Weibull modulus for 240 grit abraded rods suggests significantly less variation in fracture strength relative to the as-received and 1200 grit abraded test groups while the larger characteristic strengths of the as-received and 1200 grit abraded rods suggests the inflicted and inherent flaws were smaller than those found on the 240 grit abraded rods. Additionally, considering average flexural strength as a function of flaw size in accordance with the Griffith theory of fracture suggested lower flexural strengths were the result of larger flaw sizes. Contrastingly, considering flexural strength as a function of fracture origin size in accordance with the Griffith theory of brittle fracture revealed no apparent relationship. However, measurements of mirror radius of fracture surfaces were fairly consistent with reported values of 250 – 308 μm, yet the corresponding mirror radii were not as consistent with calculated values of 0.31 – 0.50 MPa$\sqrt{m}$. The calculated fracture toughness from Vickers indentation testing was 7.3 × 10^5 Pa$\sqrt{m}$ using linear regression analysis. Calculations from individual indentations yielded similar results.

Additionally, the presence of residual stress fields after indentation was observed using polarized, transmitted light.

2. Introduction

The flexural strength of materials is an important parameter to consider in the implementation of particular piece or mechanical device because often materials are subjected to intense internal stresses resulting from putting the rods in a state of bending. Such issues illustrate why four-point bend testing is instrumental in determining the flexural strength of a material. However, while extraction of flexural strength from individual tests may be fairly trivial, large variations in flexural strength are usually observed in brittle materials such as soda lime glass. Therefore, a two-parameter Weibull analysis of collected data provides valuable information pertaining to predictability and variation of material failure as well as material strength.

Additionally, surface flaws on test pieces can lead to increases in internal stresses and facilitate failure at much lower applied forces. Thus it is also useful to analyze the fracture surfaces of the test specimens using optical and scanning electron microscopy to determine the point of crack propagation, characterize the type of fracture, and extract multiple parameters of the fracture surface to compare for consistency between samples.

Another material parameter, plane strain fracture toughness, is important to consider regarding the ability and tendency of a crack to propagate through a material. This parameter can be estimated with relative ease by means of measuring crack lengths resulting from indentation testing. Furthermore, residual stress fields can arise after

indentation testing and it is important to analyze these strain fields by the use of transmitted light optical microscopes using crossed-polarizers to determine the tendency of the material absorb strain energy.

It is therefore the purpose of this study to characterize the mechanical properties of soda lime glass and to learn proper techniques for the mechanical testing of brittle materials.

3. Experimental Procedure

A. Preparation of Glass Rod Specimens

A group of 30 soda lime glass rods was selected at random from a particular lot of rods before being randomly divided into three groups of 10 rods. Each group was then labeled "as-received," "240 grit," or "1200 grit" and the cross-sectional diameter of each rod measured with a micrometer. The as-received rods were left unmodified, while the 240 grit and 1200 grit rods were circumferentially abraded along the mid sections using 240 and 1200 grit SiC abrasive paper respectively. Circumferential abrasion was achieved by securely wrapping a small piece of abrasive paper around each rod while completely rotating each rod 2 times.

B. Flexural Testing of Glass Specimens

An Instron 4502 machine was used along with a four-point flexural fixture to induce four-point bending in each tested rod. The dimensions of the flexural were within guidelines specifies by ASTM standard MIL-STD 1942 [1] with a length of 10 mm between consecutive points on the bending fixture. The Instron machine was calibrated to apply force to the fixture at a rate of 100 mm/min as per ASTM C1161 [2] and a computer system was used to monitor the magnitude of the applied force. When failure occurred in each rod, the applied force at failure was recorded and the pieces of the specimens were recovered for a later fractography analysis. The applied force required for failure in conjunction with the cross-sectional radius of each rod was used to calculate the strength of the rod at failure.

Data from other investigators was also compiled and compared with the data collected during this study to assess if combination of all data was reasonable. A two-parameter Weibull distribution [3] was fit to each test group of rods and the characteristic strength, Weibull modulus and error of the Weibull modulus were calculated.

Additionally the average flexural strength of the 240 grit and 1200 grit test groups were plotted versus the average flaw size to test the Griffith theory of fracture. The average flaw size was approximated to be the average particle on the abrasive paper used to abrade each respective test group

C. Fractography of Glass Specimens

Initially, the fracture surface of each rod was viewed using a Nikon SMZ optical microscope using reflected light at a magnification of 40 X. A representative optical micrograph of the fracture surface from each test group of rods was taken.

Additionally, scanning electron microscopy (SEM) was used for further analysis of the finer topographical features of each fracture surface. The fracture surfaces to be investigated were first sputter-coated with AuPd to allow for optimal use and SEM was performed using an operating voltage of 5 kV using a secondary electron detector with working distances of 9.0 – 10.0 mm. Representative scanning micrographs of selected fracture surfaces were taken and used for analysis of topographical features of the fracture surfaces.

The representative scanning electron and optical micrographs were used to estimate fracture origin sizes and mirror radii and also used to identify the mirror regions, mist regions, and hackle zones. The mirror radius and corresponding flexural strength were also used to calculate the mirror constant [4] of the material.

Additionally, to test the Griffith theory of brittle fracture [5], the size of the fracture origin for a particular rod was compared to the corresponding flexural strength of the rod.

D. Vickers Indentation Testing of Glass Slides

Indentation testing of slides of soda lime glass was performed in accordance with prior methods [6, 7]. A Buehler Micromet II tester with a Vickers diamond indentor was used to apply forces of 9.81, 4.90, 2.94, and 1.96 N to 5 separate locations respectively on the slide to create a total of 20 indentations. The indentations were spaced apart several millimeters to avoid any interaction between indentations. A Nikon SMZ optical microscope using reflected light and 40 X magnification was used to take a single micrograph of each indentation. From each micrograph, the sizes of the cracks resulting from the indentation were measured and used to estimate fracture toughness. Additional optical micrographs of selected indentations were taken using a Nikon Optiphot Metallograph optical microscope using cross-polarizers and 40 X magnification to examine the residual stress fields present in the immediate vicinity of the indentation.

An additional calculation of the fracture toughness was extracted by plotting the 3/2 power of average crack length for a given applied force versus the applied force. The slope and the error of the slope were estimated using least squares regression analysis [8] and then used to estimate the fracture toughness.

4. Results and Discussion

A. Flexural Testing

After each glass rod was tested to the point of failure and the applied force at failure, F, recorded, the flexural strength, σ_f, of each rod was calculated using the equation [9]

$$\sigma_f = \frac{2FL}{\pi \times r^3} \qquad (1)$$

where L and r were the length of 10 mm between bending points on the bending fixture, and the cross-sectional radius of the rod respectively. Calculating the flexural strength of all tested rods in this manner yielded the results presented in Table 1.

Table 1. Calculated flexural strengths of as-received and abraded rods in ascending order.

As-Received (MPa)	240 Grit (MPa)	1200 Grit (MPa)
79.1	58.2	140.
149	61.3	145
164	61.6	192
169	62.3	201
175	63.1	224
180.		
209		
212		
214		
258		

Additionally, a basic survey of all collected data revealed all investigators reported similar values for rods within as-received, 240 grit, and 1200 grit test groups.

Therefore, data from all other collaborators were considered in the determination of a two-parameter Weibull distribution for all test groups. The complete set of data used in these calculations is presented in Appendix A.

A two-parameter Weibull distribution with the least squared regression line for the as-received rods is presented in Figure 1. The calculated characteristic strength, σ_0, and Weibull modulus, m, were 191 MPa and 5.12 ± 0.07 respectively. A three-parameter Weibull analysis was not conducted for this portion of data because no threshold strength was apparent from the gathered data.

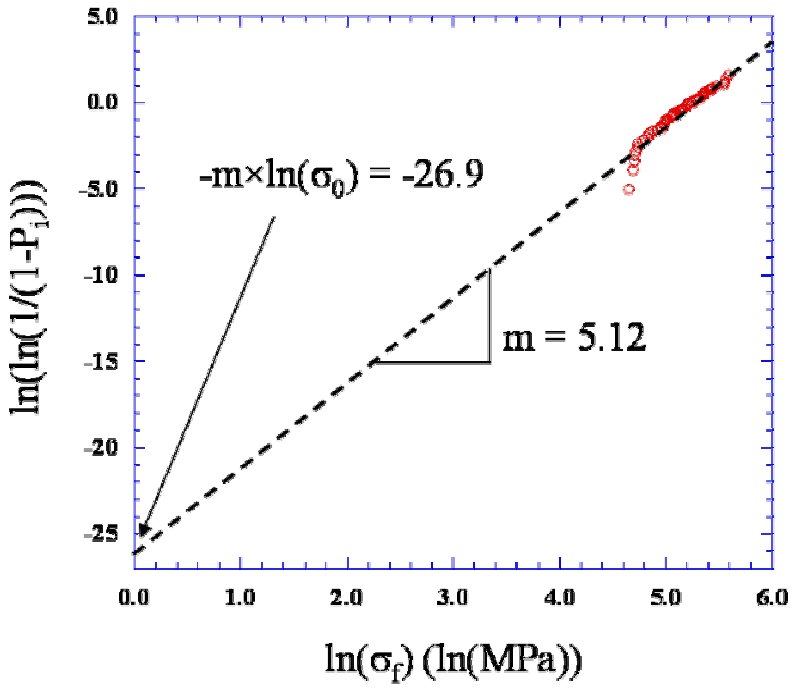

Figure 1. Two-parameter Weibull distribution of the as-received rods. The dashed line represents the least squares regression line.

The Griffith theory of fracture [5] states that the flexural strength, σ_f, of a material is proportional to the reciprocal of the square root of the size of present flaws, c.

Therefore, making the assumption that the sizes of the particles on the 240 and 1200 grit abrasive papers approximately corresponded to the flaw sizes present yielded the plot presented in Figure 2. The particle sizes of the 240 and 1200 grit abrasive papers were 53.5 and 6.5 μm [10] respectively. The calculated flexural strengths from all collaborators for each test group of abraded rods were averaged to give 61.7 and 158 MPa for 240 grit and 1200 grit test groups respectively. Although highly detailed characterization of the relationship between flexural strength and particle size was not achievable from the limited available data, it was reasonably inferred that increased flaw size lowered the corresponding flexural strength, as predicted by the Griffith theory of fracture.

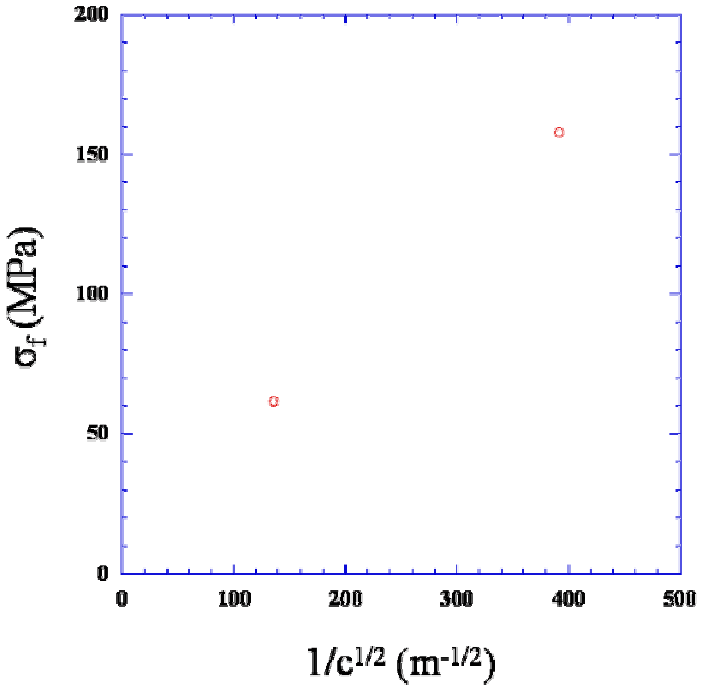

Figure 2. Flexural strength as a function of flaw size. The particle size has been approximated to be the flaw size to test the Griffith theory of brittle fracture

A two-parameter Weibull distribution with the least squared regression line for the 240 grit rods is presented in Figure 3. The calculated characteristic strength and Weibull modulus were 65.1 MPa and 9.10 ± 0.25 respectively. Similary to the as-received test group, a three-parameter Weibull analysis was not considered for this set of data because no threshold strength was apparent from the calculations.

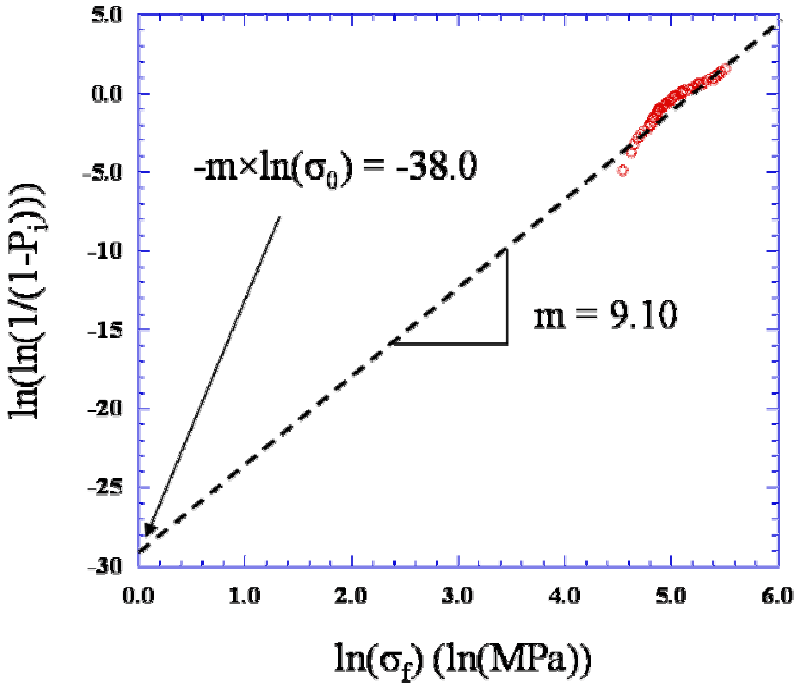

Figure 3. Two-parameter Weibull distribution of the 240 grit rods. The dashed line represents the least squares regression line.

Likewise, a two-parameter Weibull distribution with the calculated least squared regression line for the 1200 grit rods is presented in Figure 4. The calculated characteristic strength and Weibull modulus were 172 MPa and 5.44 ± 0.14 respectively. Again, a three-parameter Weibull analysis was not conducted for this set of data because no threshold strength was apparent from the calculations.

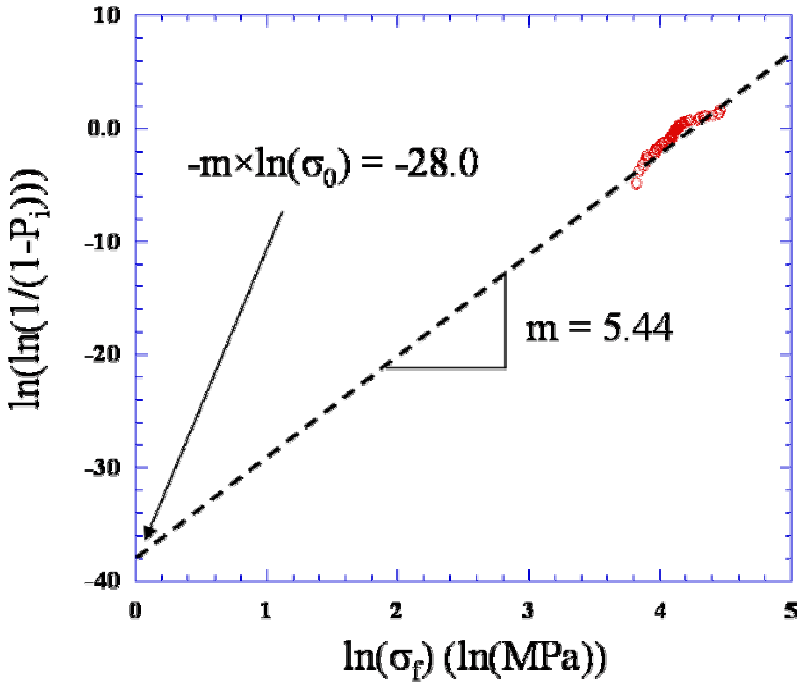

Figure 4. Two-parameter Weibull distribution of the 1200 grit rods. The dashed line represents the least squares regression line.

Observe that for the calculated flexural strengths, the characteristic strength always decreased with the use of abrasive paper with larger particles. This is predicted by the Griffith theory of fracture.

However, the relationship between abrasion treatment and Weibull modulus does not follow this relationship. The Weibull modulus was always larger for the rods abraded with larger particle abrasive paper. This suggests that the level of uniformity of abrasion among rods was greater when larger grit abrasive paper was used. This is an expected result because the as-received rods can have large variations in flexural strength due to individual processing differences and abrading as-received rods with 1200 grit paper simply did not greatly flaw the surface. In fact, no abrasion was visually observed after the 1200 grit paper was used. Therefore, the flexural strength would be primarily limited

by inherent flaws and not any impinged flaws. With the rods abraded by 240 grit paper, the flaws inflicted were significant enough to appreciably limit the influence of inherent flaws on the flexural strength. Since the abrasion treatments were fairly uniform, this explains the 240 grit paper having the largest Weibull modulus.

B. Fractography

An optical micrograph of the fracture surface of a glass rod with noted features is presented in Figure 5(a). A scanning electron micrograph of another fracture surface showing finer topographical features is also presented in Figure 5(b).

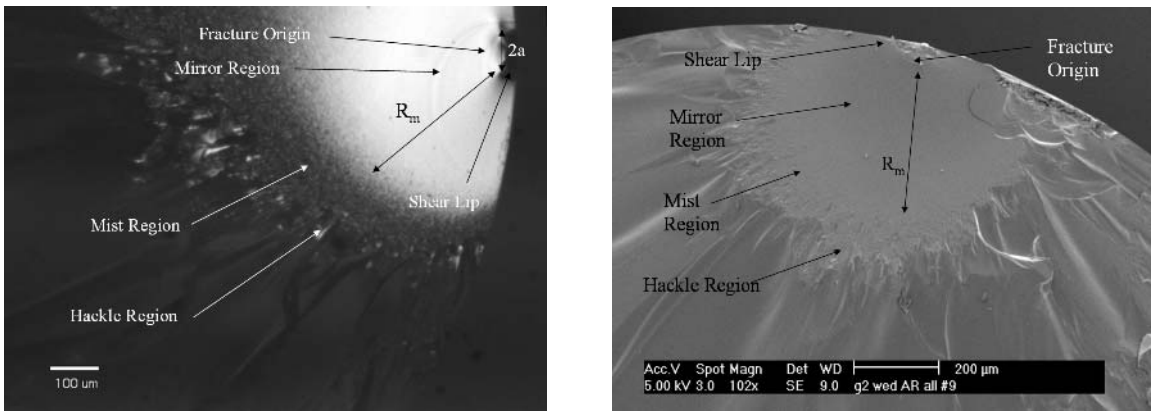

(a) **(b)**

Figure 5. (a) Optical and (b) scanning electron micrographs of the fracture surface of a glass rod. The specific features have been labeled. Observe that the origin magnitude could not be extracted from (b).

The surfaces in Figure 5 show typical brittle fractures with a clearly recognizable origins, as well as distinguishable mirror regions, mist regions, hackle regions, and mirror

radii, R_m. However, the origin size, a, was only clearly viewable in optical micrographs due to the use of reflected light.

Additionally, a possible relationship between the fracture origin size and flexural strength was explored to test the Griffith theory of brittle fracture. The Griffith theory proposes that fracture strength is proportional to the reciprocal of the square root of fracture origin size [5]. A plot of σ_f versus $1/(a^{1/2})$ is presented in Figure 6 to test this proportionality. It should be noted that the fracture origin size was only measurable for a small fraction of the total number of tested rods. This was due to a lack of consistency regarding fracture as well as incidental damage inflicted on sample fracture surfaces after testing.

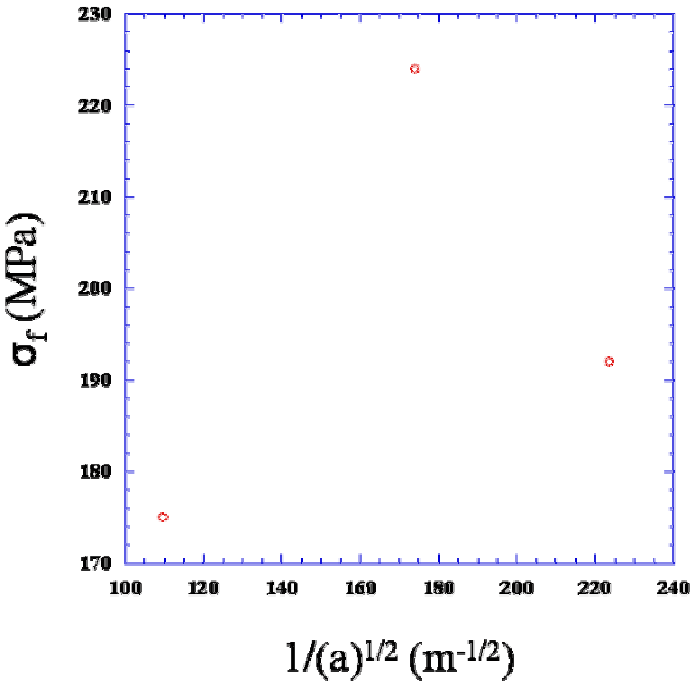

Figure 6. Plot of flexural strength versus the reciprocal of the square root of fracture origin size.

Figure 6 displays no consistent pattern regarding the relationship between fracture strength and origin size. This can be attributed to processing inconsistencies between test specimens possibly leading to flaws which altered the individual fracture strengths.

Likewise, the mirror radius of each fracture surface was measured to check for consistency of the fractures of the specimens. Similarly to the measurement of fracture origin size, only limited numbers of mirror radii were measured for this portion of the study due to incidental fracture damage caused by investigators and specimens lacking a clearly recognizable mirror radius. Discrepancies in measurements between individual investigators occurred as a result of subjective variations in determining the starting and finishing positions of the mirror radii. These variations accounted for discrepancies of approximately 10 μm in R_m measurements. After the mirror radius was measured, the mirror constant, A [4], was estimated by

$$A = \sigma_f \sqrt{R_m} \qquad (2)$$

Tabulated R_m measurements and corresponding mirror radius calculations are presented in Table 2.

Table 2. Measured fracture surface mirror radii and calculated mirror constants.

R_m (μm)	A (MPa $\sqrt{m}$)
274	0.47
300	0.50
250	0.31
308	0.28

The values of A in Table 2 show a large amount of dispersion. This can be understood by referring to Figure 6 regarding fracture strength as a function of origin size. The large variation in fracture strength can be related to variations in the processing effects on the glass as well the nature of the as-received rods to have large variations in failure strength resulting from inherent flaws.

C. Vickers Indentations

A plot of the average crack length, c, raised to the 3/2 power versus the indentation force, P, is shown in Figure 7. The slope measured from the least squares regression line is $7.9 \times 10^{-8} \pm 0.1 \times 10^{-8}$ $m^{3/2}/N$.

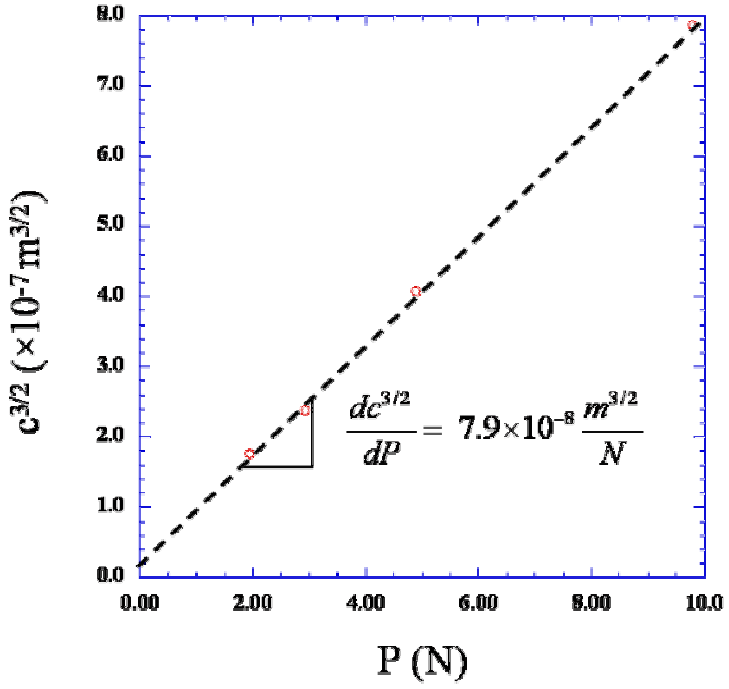

Figure 7. Average crack length raised to the 3/2 power vs. applied force. The dotted line represents the least squares regression line.

The data in Figure 7 suggests a highly linear relation ship between $c^{3/2}$ and P, and implies very little variation in fracture toughness, K_C, consistent with prior research [11].

The lengths of the cracks resulting from Vickers indentation testing were be used to calculate the fracture toughness, K_C, of the glass using the equation [11]

$$K_C = 0.016 \times \left(\frac{E}{H}\right)^{1/2} \left[\frac{P}{c^{3/2}}\right] \qquad (3)$$

where E and H are the elastic modulus and hardness respectively. For the soda lime glass being tested, the elastic modulus and hardness are 70. and 5.5 GPa respectively. Rearrangement of Equation 3 leads to the following equation

$$c^{3/2} = \frac{0.016}{K_C} \times \left(\frac{E}{H}\right)^{1/2} [P] \qquad (4)$$

Since the coefficient of P is a constant, the slope of the least squares regression line in Figure 7 is equal to this coefficient. Therefore, K_C can be calculated by

$$K_C = \frac{0.016}{\left[\frac{dc^{3/2}}{dP}\right]} \times \left(\frac{E}{H}\right)^{1/2} \tag{5}$$

Using this analysis, the calculated fracture strength is 7.3×10^5 Pa$\sqrt{m}$. Additionally, K_C values were calculated for each individual crack. The data used for these calculations are presented in Appendix B. A survey of the calculated values shows results similar to the value calculated from the slope of the least squares regression line in Figure 7. Variations in K_C exist due to small yet appreciable inconsistencies with the impact of the diamond indentor upon the glass slides. This would explain why each indentation did not always have four cracks and why the cracks are sometimes significantly different in length.

The presence of residual stress fields was also considered in this study as depicted by the optical micrograph using transmitted, polarized light in Figure 8. The bright areas correspond to places with large amounts of residual stress. Such an image is created due to the photoelasticity of the glass. Under stress, the optical axis of the glass is deflected, and thus, the ability of light to be transmitted is altered in areas of residual stress [12]. Thus, the areas with residual stress appear as bright regions on the micrographs.

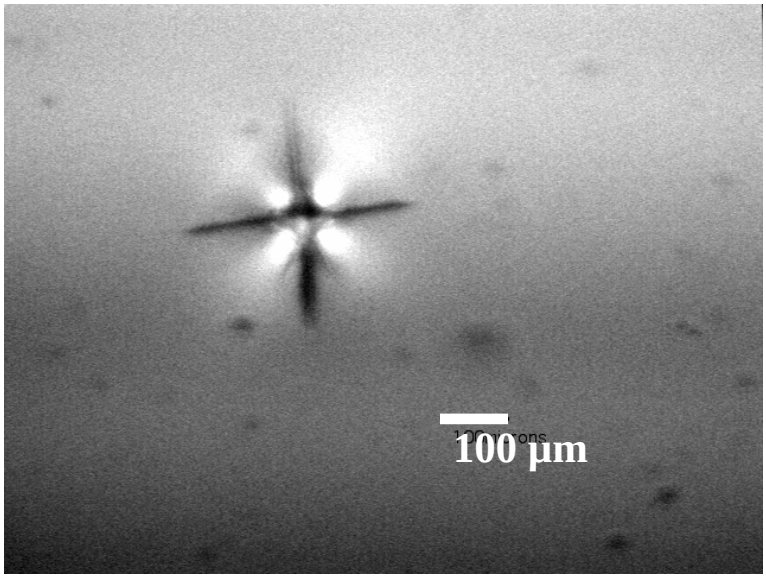

Figure 8. Optical micrograph of an indentation using transmitted polarized light. The bright areas are areas with large amounts of residual stress.

5. Conclusions

The mechanical properties of soda lime glass were tested using flexural testing, Weibull analysis, fractography, and Vickers indentation testing.

Characteristic flexural strengths of the glass rods were found to increase when the sizes of the particles used during the abrasive treatment were decreased as the Weibull analysis of as-received, 240 grit abraded, and 1200 grit abraded rods, yielded characteristic strengths of 191, 65.1, and 172 MPa respectively. Additionally, the Weibull moduli of the as-received, 240 grit, and 1200 grit test groups were 5.12 ± 0.07, 9.10 ± 0.25, and 5.44 ± 0.14 respectively, suggesting a smaller variations in flexural strength of the 240 grit and 1200 grit rods relative to the as-received rods. This observation was most likely related to considerable variations in inherent flaws of the as-

received rods, while abrasion of the rods significantly reduced the contribution of inherent flaws to the failure of the rods.

In accordance with the Griffith theory of brittle fracture, data relating flexural strengths to flaw sizes suggested lower flexural strengths were the result of larger flaw sizes. However, considering flexural strength as a function of fracture origin size produced no clear relationship. Consistent measurements of the mirror radii of fracture surfaces were obtained with values of 250 – 308 μm, yet the corresponding mirror constants showed larger variations with calculated values of 0.31 – 0.50 MPa$\sqrt{m}$. It is also noteworthy to consider that extraction of fracture origin and mirror radius measurements were not achievable for all fracture surfaces, and the limited data may be significantly influencing these variations.

The calculated fracture toughness from Vickers indentation testing was 7.3×10^5 Pa$\sqrt{m}$ using linear regression analysis with similar results obtained from calculations from individual indentations. Additionally, the use of an optical microscope using transmitted, polarized light revealed the presence of residual stress fields after indentation.

6. References

[1] American Society for Testing and Materials, Designation: MIL-STD 1942, 2002.

[2] American Society for Testing and Materials, Designation: C1161, 2002.

[3] American Society for Testing and Materials, Designation: C1239-00, 2002.

[4] T. Michalske, "Quantitative Fracture Surface Analysis," *ASM Engineered Materials Handbook, Vol. 4: Ceramics and Glasses*, ASM International, 1987.

[5] W.D. Callister, *Materials Science and Engineering: An Introduction*, 6th Edition, John Willey & Sons Inc., New York, 2002.

[6] K.E. Amin, "Toughness, Hardness, and Wear," *ASM Engineered Materials Handbook, Vol. 4: Ceramics and Glasses*, ASM International, 1987.

[7] B. Lawn and D. Marshall, *Fracture of Brittle Materials*, 2nd edition, Cambridge University Press, 1993.

[8] K. Rektorys, *Survey of Applicable Mathematics*, MIT press, pg. 1291, 1969.

[9] F.P Beer, E.R. Johnston, and J.T. Dewolf, *Mechanics of Materials*, 3rd Edition, McGraw-Hill, 2001.

[10] C.A. Johnson, "Metallographic Sample Preparation," Leco Corporation, 1977.

[11] G.R. Anstis, P. Chantikul, D.R. Lawn, and D.B. Marshall, *J. Amer. Ceram. Soc.* **64** 9 p. 533-538 (1981).

[12] H.D. Young, R.A. Freedman, *University Physics*, 10th Edition, Addison-Wesley, 2000.

7. Appendices

Appendix A: Compiled data of applied forces at fracture and cross-sectional diameters.

As-received		240 grit		1200 grit	
force (kN)	diameter (mm)	force (kN)	diameter (mm)	force (kN)	diameter (mm)
0.06163	3.1	0.03016	3.05	0.1066	3.13
0.09082	3.05	0.03041	3.08	0.1318	3.07
0.106	2.95	0.03238	3.02	0.0805	3.02
0.06387	2.94	0.02998	3.03	0.0657	2.99
0.102	2.94	0.03601	3.05	0.0897	3.08
0.09352	2.96	0.03515	3.10	0.07844	3.00
0.06181	2.98	0.03096	2.98	0.09946	3.07
0.1147	3.08	0.03027	3.16	0.1423	3.08
0.1556	3.13	0.03214	2.96	0.07919	2.93
0.1083	2.95	0.02385	2.90	0.1168	2.93
0.112	3.03	0.03585	3.07	0.08916	2.87
0.0887	3.06	0.03024	2.98	0.0858	3.11
0.106	3.03	0.03539	3.07	0.1177	3.1
0.0649	3.07	0.03044	2.93	0.06549	2.88
0.0845	3.08	0.0312	2.96	0.1246	3.05
0.0978	3.00	0.05883	3.050	0.03086	2.845
0.1423	3.00	0.06869	3.050	0.03604	3.100
0.0354	2.95	0.07251	3.020	0.03151	3.070
0.1127	2.95	0.06531	2.840	0.03247	3.035
0.1231	3.02	0.08697	3.050	0.03649	3.090
0.09028	3.01	0.11180	3.015	0.02922	2.815
0.102	3.07	0.10720	3.100	0.03661	3.090
0.1014	3.09	0.07255	3.030	0.03043	2.830
0.1162	3.05	0.07320	3.050	0.03175	3.060
0.1439	3.05	0.07386	3.045	0.02846	2.820
0.1124	3	0.03908	3.11	0.02754	2.91
0.08575	3.08	0.03081	3.1	0.09712	3
0.09214	3.06	0.03005	2.92	0.05611	2.84
0.0445	3.06	0.03543	3.12	0.07067	3.09
0.1145	3.01	0.02899	2.84	0.08193	3.01
0.10690	2.950	0.02721	3.12	0.08811	3.01
0.07395	3.055	0.03126	3	0.08100	3.01
0.08567	3.090	0.03643	3.09	0.08955	3.02
0.05543	2.935	0.03437	2.99	0.08760	3.01
0.08786	2.930	0.0351	3.1	0.09958	3.02
0.08113	2.830	0.0248	3	0.08763	3
0.01010	3.025	0.0333	3	0.0744	3
0.09889	3.050	0.0354	3.1	0.1077	3

0.15000	3.100	0.036	3.1	0.0792	3
0.06630	3.090	0.0281	3	0.0602	3.1
0.07738	3.06	0.0264	3	0.0886	3.1
0.10320	3	0.0256	3	0.0554	3.1
0.08548	3.05	0.0354	3.1	0.0637	3
0.11980	3	0.029	3	0.0761	3.1
0.06180	3.05	0.0353	3.12	0.0963	3.1
0.08888	3.11	0.0342	2.95	0.077	3.1
0.12850	3.13	0.0335	3.05	0.071	3.03
0.08899	3.14	0.0349	3.1	0.0961	3.07
0.07566	3.11	0.0309	2.97	0.0683	2.94
0.08864	3.05	0.0301	3.08	0.0915	3.04
0.0919	3	0.0363	3.08	0.0845	3.04
0.0822	2.9	0.0372	3.12	0.0971	2.95
0.0735	3.1	0.0281	2.95	0.1056	3.04
0.0922	3.1	0.0317	2.98	0.1275	3.08
0.1074	3.1	0.0436	3.11	0.117	3.04
0.1045	3	0.03165	2.91	0.0817	3.08
0.0685	2.9	0.04471	3.09	0.07978	3.07
0.138	3.1	0.04949	3.09	0.06852	3.03
0.0982	3.1	0.04363	3.07	0.07416	3.08
0.0937	3.1	0.05063	3.1	0.06507	3.06
0.1125	3.095	0.04443	3.025	0.06439	3.08
0.1082	3.04	0.0353	2.905	0.06892	3.03
0.0901	2.94	0.04061	3.05	0.1289	3.06
0.0602	3.04	0.03529	3.075	0.1025	3.02
0.0673	3.045			0.07462	3.02
0.0864	3.02			0.0618	3.07
0.0726	2.955				
0.0633	3.08				
0.0758	3.08				
0.0902	3.08				
0.1366	3.07				
0.1228	3.115				
0.1246	3.015				
0.1018	3.06				
0.06711	2.865				
0.07722	2.98				
0.1318	3.1				
0.0988	2.99				
0.1187	2.85				
0.07783	3.01				

Appendix B: Compiled data of crack lengths and applied indentation forces.

applied force (N)	indentation number	crack length (microns) and orientation			
1.96		left	top	right	bottom
	1	31.3	31.2	30.4	
	2	27.6	30.6		30.1
	3		28.9	18.6	26.3
	4	28.8	32.1		30.1
	5	39.4	42.4	38.6	35.3
2.94		left	top	right	bottom
	1	37.4	40.6	37.2	35.3
	2	41.8	42.1	40.7	40.5
	3	38.8	38.5	33	21.3
	4	41.9	41.5	40	40
	5	41.6	40.5	35.3	39.5
4.9		left	top	right	bottom
	1	53.8	52.1	55.6	50
	2	55.7	55.7	55.7	52.3
	3	53.8	55.6	54.1	50
	4	57.4	57.4	55.6	59.8
	5	57.5	55.7	54	58.5
9.8		left	top	right	bottom
	1	87.2	87	84.5	86.6
	2	87.8	84.5	89.2	86.3
	3	86.7	85	83.4	81.9
	4	88	89.2	74.3	76.2
	5	88.8	92.3	84.3	79.5